

Georg Vohl,^{a,b} Ruslan
Nedielkov,^c Björn Claussen,^b
Marco S. Casutt,^a Thomas
Vorburger,^d Kay Diederichs,^c
Heiko M. Möller,^{c,‡} Julia
Steuber^d and Günter Fritz^{a*}

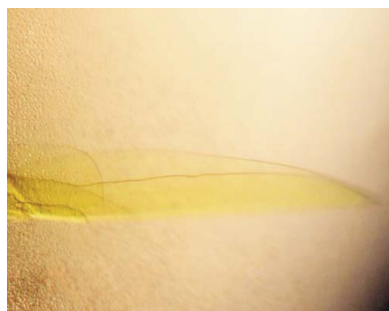
^aInstitute for Neuropathology, University of Freiburg, Breisacher Strasse 64, 79106 Freiburg, Germany, ^bHermann-Staudinger-Graduate School, University of Freiburg, Hebelstrasse 27, 79104 Freiburg, Germany, ^cDepartment of Chemistry and Research School Chemical Biology, University of Konstanz, Universitätsstrasse 10, Konstanz, 78457, Germany, and ^dDepartment of Microbiology, University of Hohenheim, 70599 Garbenstrasse 30, Stuttgart, Germany

‡ Current address: Institute of Chemistry, University of Potsdam, Karl-Liebknecht-Strasse 24-25, 14476 Potsdam, Germany.

Correspondence e-mail:
guenter.fritz@uniklinik-freiburg.de

Received 11 March 2014

Accepted 1 May 2014



© 2014 International Union of Crystallography
All rights reserved

Crystallization and preliminary analysis of the NqrA and NqrC subunits of the Na⁺-translocating NADH:ubiquinone oxidoreductase from *Vibrio cholerae*

The Na⁺-translocating NADH:ubiquinone oxidoreductase (Na⁺-NQR) from *Vibrio cholerae* is a membrane protein complex consisting of six different subunits NqrA–NqrF. The major domains of the NqrA and NqrC subunits were heterologously expressed in *Escherichia coli* and crystallized. The structure of NqrA_{1–377} was solved in space groups *C*222₁ and *P*2₁ by SAD phasing and molecular replacement at 1.9 and 2.1 Å resolution, respectively. NqrC devoid of the transmembrane helix was co-expressed with ApBE to insert the flavin mononucleotide group covalently attached to Thr225. The structure was determined by molecular replacement using apo-NqrC of *Parabacteroides distasonis* as search model at 1.8 Å resolution.

1. Introduction

Vibrio cholerae is a Gram-negative bacterium that lives in brackish or sweet water environments. Strains of *V. cholerae* carrying pathogenicity islands infect the human gut and cause the disease cholera. *V. cholerae* maintains a Na⁺ gradient at its cytoplasmic membrane that drives substrate uptake, motility and efflux of antibiotics.

The Na⁺ motive force is generated by NADH:ubiquinone oxidoreductase (Na⁺-NQR), a membrane protein complex of about 220 kDa coupling the exergonic oxidation of NADH to the transport of Na⁺ across the cytosolic membrane. It has been shown that the presence of Na⁺-NQR modulates virulence-factor expression in *V. cholerae* (Häse & Mekalanos, 1999). Notably, Na⁺-NQR is a respiratory enzyme in many other pathogens such as *Yersinia pestis* (Black Death), *Klebsiella pneumoniae* (pneumonia) and *Neisseria meningitidis* (meningitis).

Na⁺-NQR has a function analogous to mitochondrial complex I but exhibits a completely different architecture. It consists of six subunits NqrA–NqrF. NqrB, NqrD and NqrE are integral membrane proteins, NqrC has been predicted to be anchored by two transmembrane helices (Duffy & Barquera, 2006) and NqrF is anchored by a single transmembrane helix (Duffy & Barquera, 2006; Türk *et al.*, 2004), whereas NqrA is devoid of a membrane anchor and is tightly attached to the membrane-bound subunits (Duffy & Barquera, 2006).

To date, there is no structural information available for Na⁺-NQR from *V. cholerae*. We have crystallized a major domain of the NqrF subunit (Tao *et al.*, 2006) and we recently also succeeded in crystallization of the entire Na⁺-NQR complex (Casutt *et al.*, 2010). Structures of an NqrF subdomain from *Porphyromonas gingivalis* (PDB entry 2r6h; Midwest Center for Structural Genomics, unpublished work) and of a soluble domain of NqrC from *Parabacteroides distasonis* (PDB entry 3lwx; Joint Center for Structural Genomics, unpublished work) have been deposited in the PDB. However, the covalently linked flavin mononucleotide (FMN) cofactor was lacking. The crystals of the NqrF subdomain diffracted well, allowing the determination of a high-resolution structure. Unfortunately, the crystals of the entire Na⁺-NQR complex diffracted to just beyond 4 Å resolution. At this resolution many molecular details were still not resolved. We therefore aimed to complement our low-resolution analysis with high-resolution structures of further single subunits. Here, we report the crystallization of the major domains of NqrA and

NqrC. The structures of the subunits were determined by SAD phasing and molecular replacement, respectively.

2. Materials and methods

2.1. Cloning, protein expression and purification

2.1.1. Isolation and analysis of C-terminally truncated NqrA. Full-length NqrA comprising residues 1–446 was expressed and purified as described previously (Nediakov *et al.*, 2013; Casutt *et al.*, 2011) using immobilized metal-ion chromatography (IMAC) and size-exclusion chromatography. Although protease inhibitors had been added to the cell-free extracts, the protein eluting from IMAC showed two further bands at lower molecular masses of approximately 38 and 40 kDa, suggesting a C-terminal proteolytic truncation. A smaller fragment corresponding to the cleaved-off C-terminus was not observed. In order to identify the proteolysis product, NqrA and truncated NqrA were subjected to anion-exchange chromatography using a SOURCE 15Q column (10 × 50 mm) connected to an ÄKTA chromatography system (GE Healthcare). The sample was dialyzed against 20 mM Tris–HCl pH 8.0 and applied onto the column equilibrated in the same buffer. Bound proteins were eluted in a linear gradient to 20 mM Tris–HCl, 1.0 M NaCl pH 8.0 and fractions were analyzed on SDS–PAGE. The cysteines of samples were blocked in SDS–PAGE sample buffer containing 125 mM iodoacetamide for 20 min at room temperature and the reaction was stopped by adding 70 mM DTT. Bands containing truncated NqrA were excised and subjected to mass-spectrometric analysis as described previously (Casutt *et al.*, 2012). The analysis revealed two major fragments of NqrA comprising residues 2–370 and 2–377. Structure prediction (Kelley & Sternberg, 2009) suggested that NqrA forms two domains: an N-terminal domain consisting of residues 1–378 and a short C-terminal domain consisting of residues 379–446. Since crystallization trials of full-length NqrA had not been successful, we decided to produce a C-terminally truncated variant of NqrA.

2.1.2. Cloning of NqrA_{1–377}. For expression of NqrA_{1–377} a synthetic cDNA with codons optimized for expression in *Escherichia coli* was obtained from a commercial supplier (GenScript). The cDNA was flanked with restriction sites for *NdeI* and *XhoI* at the 5' and 3' ends, respectively, and was cloned *via* the same sites into pET-15b (Novagen), yielding pET-15b-NqrA_{1–377}. The resulting gene encodes for NqrA_{1–377} with an N-terminal thrombin cleavable hexahistidine tag. After cleavage with thrombin the protein has three additional residues, G-S-H, at the N-terminus.

2.1.3. Expression and purification of NqrA_{1–377}. For heterologous expression of NqrA_{1–377}, the plasmid pET-15b-NqrA_{1–377} was transformed into *E. coli* Tuner (DE3) cells (Novagen). Expression cultures for NqrA_{1–377} were grown in shaking culture in baffled flasks at 37°C in DYT supplemented with 50 mM Na₂HPO₄, 0.2% glucose, 100 µg ml⁻¹ ampicillin until an OD_{600 nm} of 0.8 was reached. Expression was induced by the addition of 1 mM IPTG and the culture was further incubated for 5 h at 30°C. Cells were harvested by centrifugation for 15 min at 8000g. Typically, 10 g wet weight cells were suspended in 20 ml of ice-cold 50 mM sodium phosphate, 300 mM NaCl pH 8.0, supplemented with approximately 2 mg DNase I, 5 mM MgCl₂ and EDTA-free cOmplete protease inhibitor (Roche). The cells were lysed by two passages through a French pressure cell at 137 MPa. Cell debris was removed by centrifugation for 1 h at 30 000g and 4°C. All subsequent chromatographic steps were carried out at 4°C on an FPLC system (GE Healthcare). The supernatant was diluted twofold with 50 mM sodium phosphate, 300 mM NaCl, 5% glycerol, 30 mM imidazole pH 8.0 and loaded onto

an Ni Sepharose Fast Flow column (10 × 120 mm) equilibrated in the same buffer. The column was washed with the same buffer until the absorption at 280 nm reached the baseline level and the bound protein was eluted with 50 mM sodium phosphate, 300 mM NaCl, 5% glycerol, 250 mM imidazole pH 8.0. For cleavage of the His₆ tag 0.5 U thrombin per milligram of NqrA and 2 mM CaCl₂ were added, followed by incubation at room temperature for 16 h. Uncleaved protein and the His₆ tag were removed by passing the sample over an Ni Sepharose Fast Flow column. Prior to anion exchange on a SOURCE 15Q column (10 × 90 mm), the sample was concentrated by ultrafiltration (30 kDa cutoff, Merck Millipore), diluted fivefold with 10 mM HEPES–NaOH, 5% glycerol pH 8.0 and loaded onto the column equilibrated in the same buffer. Bound protein was eluted in a linear gradient to 10 mM HEPES–NaOH, 5% glycerol, 300 mM NaCl pH 8.0. Fractions containing NqrA_{1–377} were combined and loaded onto a Superdex 75 (16/60) column (GE Healthcare) equilibrated in 10 mM HEPES–NaOH, 5% glycerol, 300 mM NaCl pH 8.0 and eluted in the same buffer. The pure protein was concentrated by ultrafiltration (30 kDa cutoff, Merck Millipore) to 15 mg ml⁻¹ and aliquots were flash-frozen in liquid nitrogen and stored at –80°C.

2.1.4. Cloning, expression and purification of NqrC_{33–257}. For expression of NqrC devoid of the N-terminal transmembrane helix, a cDNA encoding residues 33–257 was synthesized by a commercial supplier (GenScript). Furthermore, the cDNA encoded an N-terminal hexahistidine tag followed by a HR3C protease recognition site at the 5' end. After cleavage the mature protein has four additional residues G-P-G-H at the N-terminus. The cDNA was flanked by *NcoI* and *XhoI* sites at the 5' and 3' ends, respectively, and was cloned into pET-15b using the same sites, yielding pET-15b-NqrC_{33–257}. For co-expression of ApbE, which catalyzes the covalent linkage of FMN to Thr225 of NqrC (Bertsova *et al.*, 2013), the sequence of the *apbE* gene from *V. cholerae* (accession No. NC_009457.1; GeneID 5135954) was used to design a synthetic cDNA fragment lacking the leader sequence encoding amino-acid residues 51–367. The cDNA was flanked at the 5' end with an *NcoI* site and at the 3' prime end with a cDNA encoding the residues for a HR3C protease-cleavable *Strep*-tag, two stop codons and a *PacI* restriction site. A silent mutation was introduced within the *apbE'* sequence to eliminate an *NcoI* restriction site. The desired fragment was obtained by restriction with *NcoI* and *PacI* and cloned into pACYC-Duet-1 (Merck Millipore), to yield pACYC-*apbE'*, which confers chloramphenicol resistance. Expression of *ApbE'* containing a C-terminal *Strep*-tag was controlled by the lac promoter. All constructs were confirmed by sequencing.

Both plasmids were transformed into *E. coli* BL21(DE3) cells. Expression cultures for NqrC_{33–257} were grown in shaking culture in baffled flasks at 37°C in DYT supplemented with 50 mM NaHPO₄, 0.2% glucose, 100 µg ml⁻¹ ampicillin until an OD_{600 nm} of 1.0 was reached. Expression was induced by the addition of 0.5 mM IPTG and after 5 h at 37°C the cells were harvested by centrifugation at 8000g. The cells were lysed using a French press and after centrifugation at 30 000g for 1 h the supernatant was diluted threefold with 50 mM sodium phosphate, 300 mM NaCl, 5% glycerol, 10 mM imidazole pH 8.0 and loaded onto an Ni Sepharose Fast Flow column (10 × 120 mm). The column was washed with 50 mM sodium phosphate, 300 mM NaCl, 5% glycerol, 20 mM imidazole pH 8.0 until the absorption at 280 nm reached the baseline level and bound His₆-NqrC_{33–257} was eluted with 50 mM sodium phosphate, 300 mM NaCl, 5% glycerol, 250 mM imidazole pH 8.0. The His₆ tag was cleaved by digestion with His₆-tagged PreScission protease (Basters *et al.*, 2014) at 4°C for 14 h. The His₆ tag, undigested protein and His₆-tagged PreScission protease were removed by passing the sample over an Ni

Sepharose Fast Flow column. The flowthrough containing NqrC_{33–257} was concentrated by ultrafiltration (10 kDa cutoff, Merck Millipore) and applied onto a Superdex 75 (26/60) column equilibrated in 10 mM HEPES–NaOH, 5% glycerol, 300 mM NaCl pH 7.5 and eluted with the same buffer. The pure protein was concentrated by ultrafiltration to 15 mg ml^{−1} and aliquots were flash-frozen in liquid nitrogen and stored at −80°C.

NqrC_{33–257} expressed in the absence of ApbE yielded colourless, FMN-free protein that formed a dimer and a minor fraction of a monomeric species as judged from size-exclusion chromatography. Cytoplasmic co-expression of ApbE resulted in the covalent insertion of FMN. Size-exclusion chromatography yielded two peaks containing NqrC_{33–257}; about 80% of the NqrC_{33–257} eluted at a volume corresponding to monomeric protein, whereas about 20% eluted at a smaller volume corresponding to a dimer (Fig. 1a). Comparison of the ratios at 280/400 nm for both fractions revealed an

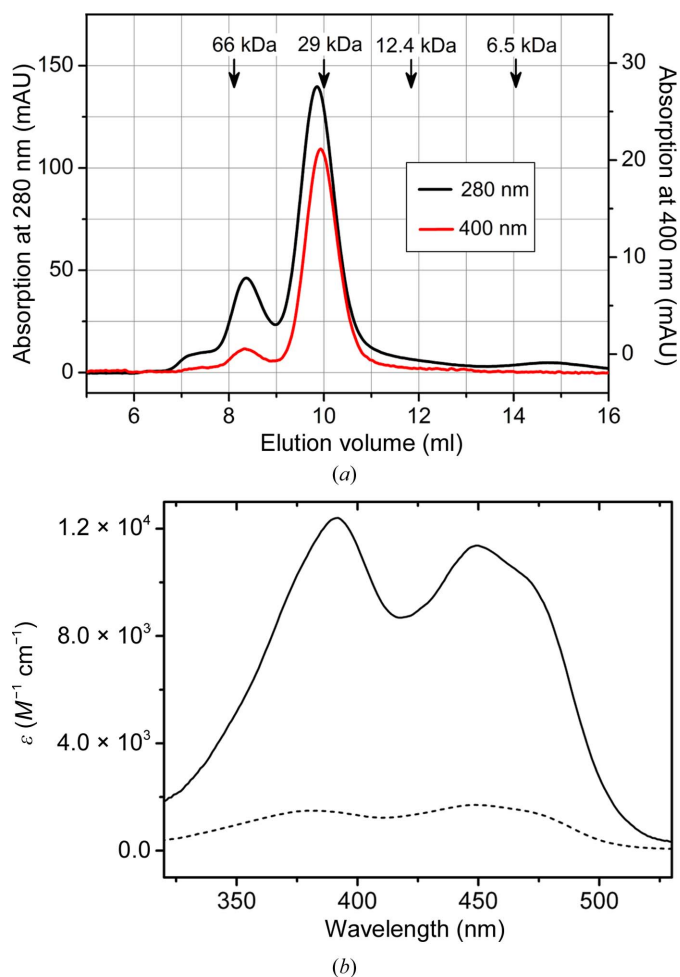


Figure 1

Molecular properties of NqrC_{33–257}. (a) Analytical size-exclusion chromatogram of NqrC_{33–257} after the Ni Sepharose Fast Flow column. The absorption at 280 nm (black curve) and at 400 nm (red curve) is shown. The protein elutes in two peaks; the first small peak corresponds to approximately dimeric NqrC_{33–257} and the second major peak to monomeric NqrC_{33–257}. Elution volumes of marker proteins are indicated by arrows. The first peak exhibited a much lower ratio at 400/280 nm compared to the second major peak. (b) Absorption spectra of monomeric NqrC_{33–257} (solid line) and dimeric NqrC_{33–257} (broken line). Monomeric NqrC_{33–257} exhibited an extinction coefficient $\epsilon_{450\text{ nm}} = 11\,400\text{ M}^{-1}\text{ cm}^{-1}$, whereas an $\epsilon_{450\text{ nm}} = 1700\text{ M}^{-1}\text{ cm}^{-1}$ was determined for dimeric NqrC_{33–257}. Calculating the FMN content using the extinction coefficient $\epsilon_{450\text{ nm}} = 12\,500\text{ M}^{-1}\text{ cm}^{-1}$ of free FMN shows that the FMN content in the monomeric species is >90%, whereas the FMN content in the dimeric species is ~14%.

almost tenfold higher flavin content for monomeric NqrC_{33–257} than for the dimeric species. Absorption spectra of both samples and calculation of the extinction coefficient confirmed these data (Fig. 1b). The specific extinction coefficients at 450 nm were $\epsilon_{450\text{ nm}} = 11\,400\text{ M}^{-1}\text{ cm}^{-1}$ for monomeric NqrC_{33–257} and $1700\text{ M}^{-1}\text{ cm}^{-1}$ for the dimeric fraction. Comparing these values with the extinction coefficients of free FMN $\epsilon_{450\text{ nm}} = 12\,500\text{ M}^{-1}\text{ cm}^{-1}$ shows that the monomeric species of NqrC_{33–257} represents holo NqrC_{33–257}, whereas the multimeric species contains sub-stoichiometric amounts of FMN.

2.2. Protein crystallization

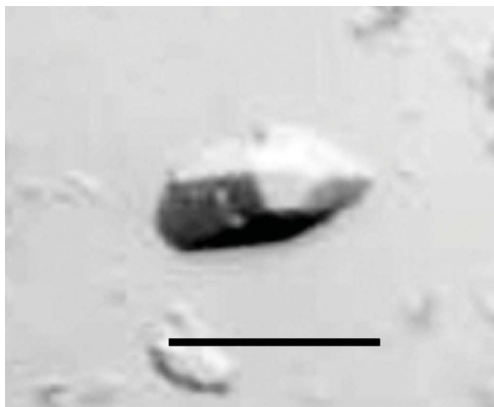
Initial crystallization trials for all proteins were performed using a Phoenix pipetting robot (Art Robbins Instruments) using the sitting-drop vapour-diffusion method with 96-well plates. For each condition three different drops were set up by mixing 200 nl protein solution with 200 nl buffer, 200 nl protein solution with 300 nl buffer or 300 nl protein solution with 200 nl buffer and were equilibrated against 50 μl crystallization buffer. Protein concentration was varied between 5 and 15 mg ml^{−1}. Crystallization trials were performed at 4 and 20°C using different commercial and homemade crystallization screens. Trials with full-length NqrA_{1–446} never yielded any crystals. We had observed that the C-terminus of NqrA was prone to proteolytic cleavage, indicating that this part of the protein might be rather flexible and therefore accessible to proteases. The presence of the flexible domain might also obstruct crystal formation, as observed for full-length NqrA_{1–446}. We therefore continued with trials using NqrA_{1–377}. The protein was thawed on ice and 15 mM DTT was added prior to crystallization. Crystals were observed after 4–6 d in two similar conditions. Small, elongated, rhomboid-shaped crystals of approximate dimensions 20 × 20 × 60 μm were detected in drops set up at 20°C with 200 nl protein solution at 10 mg ml^{−1} and 200 nl 0.1 M HEPES–NaOH pH 7.5, 25% PEG 3350, 0.2 M NaCl (Fig. 2a). In contrast, cuboid crystals were detected with 0.1 M Tris–HCl pH 8.5, 25% PEG 3350, 0.2 M Li₂SO₄ (Fig. 2b) as the crystallization buffer. In refined screens the pH, the PEG concentration and the inorganic salt, and the type of crystallization setup were varied. However, crystals were only obtained in conditions that were very similar to the initial conditions and only in 96-well plates, not in 24-well sitting-drop or hanging-drop plates. By increasing the drop size to 800 nl cuboid crystals grew to a maximum size of 50 × 100 × 100 μm at a pH between 7.5 and 8.5, 24–26% PEG 3350, 0.2 M Li₂SO₄. Crystals were mounted in nylon loops (Hampton Research) and flash-cooled in liquid nitrogen without any further addition.

In crystallization trials using apo NqrC_{33–257}, both the monomeric and the dimeric fraction yielded no diffracting crystals. Initial screens using monomeric holo NqrC_{33–257} also yielded no crystals when the protein was still in the same buffer as eluted from size-exclusion chromatography. However, crystallization was successful when the buffer was exchanged to 10 mM Tris pH 8.0 by passing the sample over an NAP-5 column (GE Healthcare) equilibrated in the same buffer. Small yellow crystals of approximately 5 × 5 × 20 μm in size were obtained after 7 d in drops set up with 200 nl protein solution and 200 nl 0.1 M Tris pH 8.5, 12.5% PEG 1000, 12.5% PEG 3350, 12.5% MPD, 0.03 M NaF, 0.03 M NaBr, 0.03 M NaI. In further trials, 2 μl protein solution was mixed with 2 μl buffer and equilibrated against 500 μl buffer in hanging-drop trials in EasyXtal 15-well plates (Qiagen) or sitting-drop trials in Cryschem M plates (Hampton Research). Varying the pH between 8 and 9 and the PEG 1000/PEG 3350/MPD concentrations between 9 and 15%, very thin plate-like crystals of NqrC_{33–257} with dimensions 300 × 400 × 5 μm were obtained (Fig. 2c). The fragile crystals were mounted in nylon loops

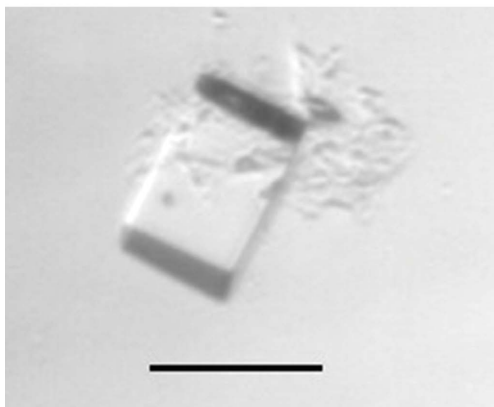
(Hampton Research) and directly flash-cooled in liquid nitrogen. No further addition was required for cryoprotection.

2.3. Data collection, processing and structure solution

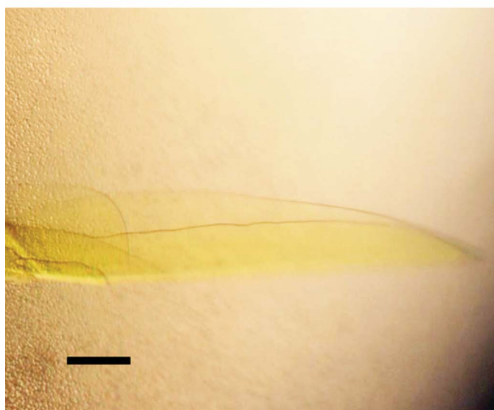
Data collection was carried out on beamlines X06SA and X06DA at the Swiss Light Source (Villigen, Switzerland) equipped with a MAR 225 CCD, PILATUS 6M or PILATUS 2M detector (Dectris). The diffraction data were processed with the *XDS* package (Kabsch, 2010). Despite their small size (Fig. 2*a*), the crystals of NqrA_{1–377} diffracted well using a small beam size of 20 × 20 μm at the micro-



(a)



(b)



(c)

Figure 2
Crystals of NqrA_{1–377} and NqrC_{33–257}. (a) Crystal form 1 of NqrA_{1–377}. (b) Crystal form 2 of NqrA_{1–377}. (c) Crystal of holo NqrC_{33–257}. The scale bar in each picture corresponds to 50 μm.

Table 1
Data-collection and refinement statistics for NqrA_{1–377}.

Values in parentheses are for the outer shell.

Crystal	Native 1	Native 2	K ₂ PtCl ₄ derivative
X-ray source	X06SA MD2, SLS	X06DA, SLS	X06DA, SLS
Wavelength (Å)	1.0	1.03	1.06
Detector	MAR 225 CCD	Dectris PILATUS 2M	Dectris PILATUS 2M
Total rotation range (°)	200	360	1200
Resolution range (Å)	50–2.1 (2.2–2.1)	50–1.9 (2.0–1.9)	50–2.4 (2.4–2.2)
Space group	<i>P</i> 2 ₁	<i>C</i> 222 ₁	<i>C</i> 222 ₁
Unit-cell parameters (Å, °)	<i>a</i> = 56.2, <i>b</i> = 81.7, <i>c</i> = 85.1, β = 92.7°	<i>a</i> = 78.1, <i>b</i> = 83.5, <i>c</i> = 101.7	<i>a</i> = 78.7, <i>b</i> = 83.6, <i>c</i> = 101.4
No. of reflections	188843 (24607)	344684 (43713)	748132 (158837)
No. of unique reflections	44981 (5832)	26419 (3683)	17305 (3893)
Multiplicity	7.7 (4.2)	13.0 (11.8)	43.2 (40.8)
<i>I</i> / <i>σ</i> (<i>I</i>)	8.2 (1.3)	27.4 (4.4)	22.8 (1.8)
Completeness (%)	99.9 (99.9)	99.5 (99.1)	99.9 (99.7)
<i>R</i> _{merge} † (%)	12.9 (126.6)	9.6 (189.2)	18.3 (275)
<i>R</i> _{meas} ‡ (%)	14.8 (144.9)	10.0 (197.6)	18.5 (278)
CC* §	99.7 (56.5)	99.9 (58.4)	100.0 (78.8)
No. of molecules per asymmetric unit	2	1	1
Matthews coefficient (Å ³ Da ^{−1})	2.41	2.05	2.05
Solvent content (%)	49.1	40.1	40.1
<i>R</i> _{work} (%)	20.1 (34.5)	17.0 (29.0)	
<i>R</i> _{free} (%)	23.5 (37.6)	19.6 (33.5)	
Average <i>B</i> factors (Å ²) from <i>phenix.refine</i>			
All atoms	48.7	39.8	
Protein	48.9	39.3	
Solvent	45.0	42.4	

$$\dagger R_{\text{merge}} = \frac{\sum_{hkl} \sum_i |I_i(hkl) - \langle I(hkl) \rangle|}{\sum_{hkl} \sum_i I_i(hkl)} \quad \ddagger R_{\text{meas}} = \frac{\sum_{hkl} \{ [N(hkl) / (N(hkl) - 1)]^{1/2} \sum_i |I_i(hkl) - \langle I(hkl) \rangle| \}}{\sum_{hkl} \sum_i I_i(hkl)} \quad \S \text{CC}^* = [2\text{CC}_{1/2} / (1 + \text{CC}_{1/2})]^{1/2} \text{ (Karplus \& Diederichs, 2012).}$$

focus setup of X06SA (Fig. 3*a*). The elongated rhomboid crystals belonged to space group *P*2₁, with unit-cell parameters *a* = 56.2, *b* = 81.7, *c* = 85.1 Å, α = γ = 90°, β = 92.7°, and diffracted to 2.1 Å resolution (Table 1) applying the CC_{1/2} criterion as defined by Karplus & Diederichs (2012). The cuboid crystals of NqrA_{1–377} belonged to space group *C*222₁, with unit-cell parameters *a* = 78.1, *b* = 83.5, *c* = 101.7 Å, α = β = γ = 90°, and diffracted to 1.9 Å resolution (Table 1). Since no structure homologous to NqrA has yet been reported, phase determination by molecular replacement was not possible. Therefore, we prepared heavy-atom soaks for MIRAS or SAD phasing. We selected a total of nine different Pt, Hg and Au salts for soaking experiments. In order to shorten the soaking time (10 min), we used rather high concentrations of heavy atoms ranging between 40 and 200 mM. A derivative with K₂PtCl₄ still diffracted to 2.2 Å resolution and the data exhibited a good anomalous signal. Several data sets collecting wedges of 6° with inverse-beam orientation with a total φ of 1200° were recorded, integrated with *XDS* (Kabsch, 2010) and scaled using *XSCALE* (Kabsch, 2010). The heavy-atom substructure was determined with *HySS* (Grosse-Kunstleve & Adams, 2003), phases were determined using the *Phaser* (McCoy *et al.*, 2007) SAD module and an initial model was built using *RESOLVE* (Terwilliger, 2004). The *AutoSol* pipeline from the *PHENIX* package (Adams *et al.*, 2010) was used to run the programs. After solvent flattening with *Parrot* (Zhang *et al.*, 1997) the initial model was extended with *Buccaneer* (Cowtan, 2006) and refined against the native data. The model was used to determine the structure of NqrA_{1–377} in the crystals of space group *P*2₁ by molecular replacement using *Phaser* (McCoy *et al.*, 2007).

The very thin NqrC_{33–257} crystals showed highly anisotropic diffraction dependent on the orientation of the crystals in the X-ray beam. When the X-ray beam crossed the short section of the crystals, a clear diffraction pattern with spots up to a resolution of 1.7 Å was observed (Fig. 3*b*). However, diffraction of the crystals oriented with the long side to the X-ray beam resulted in poor diffraction with smeared spots and a maximum resolution of 2.5 Å (Fig. 3*c*). The crystals belonged to space group *P*2₁, with unit-cell parameters $a = 46.7$, $b = 41.7$, $c = 61.4$ Å, $\alpha = \gamma = 90$, $\beta = 107.7^\circ$. For molecular-replacement trials a polyserine homology model of NqrC_{33–257} from *V. cholerae* was built using the structure of NqrC from *Parabacteroides distasonis* (PDB entry 3lwx) as template with

MODELLER (Eswar *et al.*, 2006) and *MOLEMAN* (Kleywegt *et al.*, 2001). Molecular-replacement trials were performed using *Phaser* and the Z-score of the translation function (TFZ) was 6.5 with a final LLG of 261 indicating a solution. However, refinement trials using *phenix.refine* or *REFMAC5* (Murshudov *et al.*, 2011) with different refinement strategies yielded an R_{work} of 46% and an R_{free} of 55%. We presumed that either the molecular-replacement solution is not correct or that the observed anisotropic diffraction contributes to the high R factors in refinement.

In an initial trial, we reintegrated only those images that showed well defined spots. This data set showed lower completeness but lower R_{merge} and R_{meas} (Table 2). Using the same strategy in *Phaser* the solution was not as clear as in the previous runs, with TFZ = 6.3 and LLG = 121. However, refinement in *REFMAC5* using the jelly-body option yielded an R_{work} of 41% and an R_{free} of 48% for the polyserine model, indicating a correct solution. In a second trial, we used *phenix.rosetta_refine* (DiMaio *et al.*, 2013) to refine the initial molecular-replacement model using the complete data as in the previous runs. In contrast to *phenix.refine* or *REFMAC5*, refinement in *phenix.rosetta_refine* yielded an R_{work} of 39% and an R_{free} of 48%. The initial model from *phenix.rosetta_refine* was used as input for *ARP/wARP* (Langer *et al.*, 2008) automatic model building, which built a large portion of the molecule with an R_{work} of 24% and R_{free} of 30%. This indicates that the Rosetta force field implemented in *phenix.rosetta_refine* originally described to improve refinement at low resolution also copes well with poor initial molecular-replacement models. After manual rebuilding with *Coot* (Emsley & Cowtan, 2004) and refinement with *phenix.refine* (Afonine *et al.*, 2012) the final model of NqrC_{33–257} displayed an R_{work} of 18.4% and an R_{free} of 20.9%, respectively.

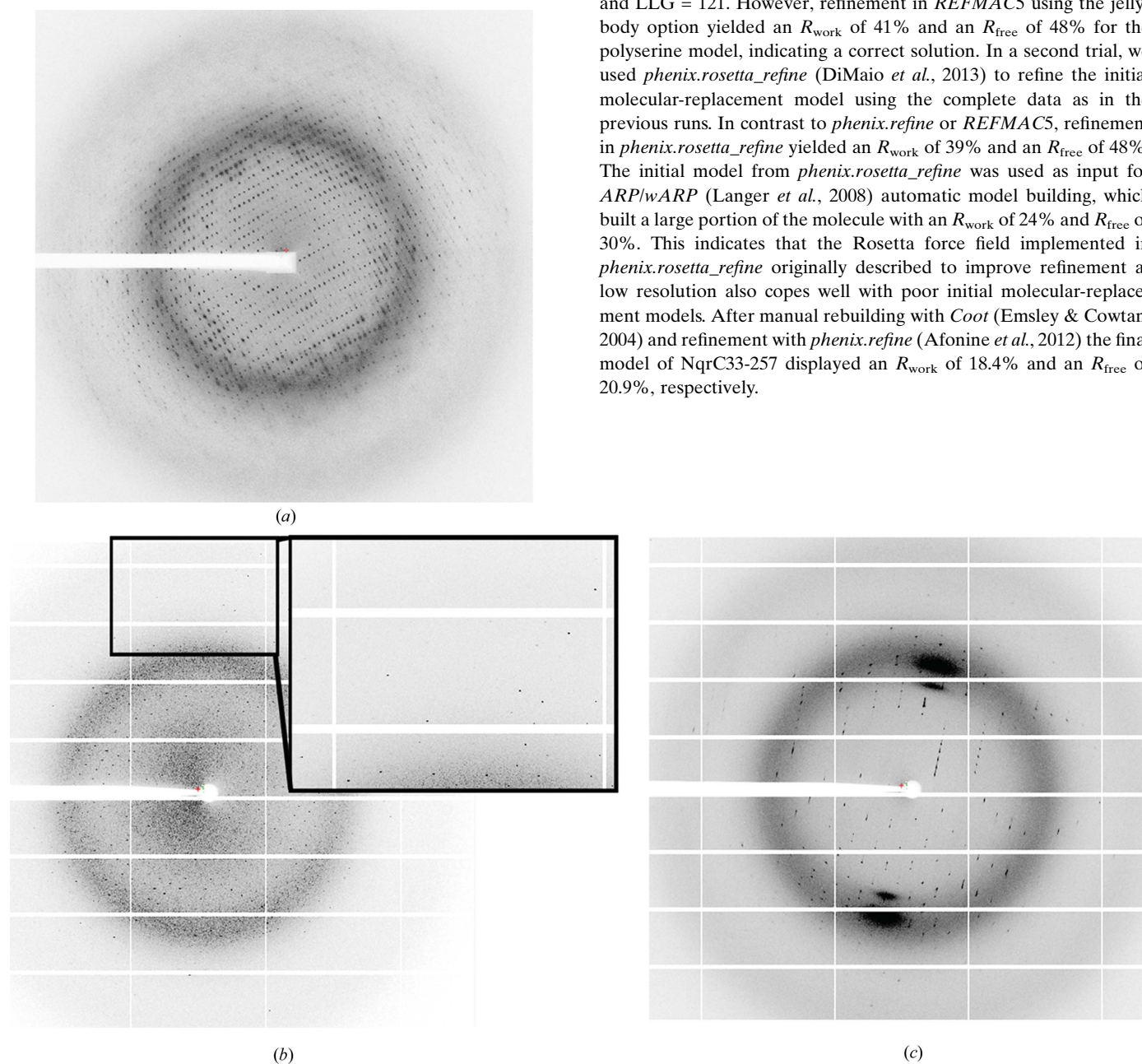


Figure 3 Diffraction pattern of crystals of NqrA_{1–377} and NqrC_{33–257}. (a) Diffraction pattern of crystals of NqrA_{1–377} belonging to space group *C*222₁. The resolution at the image border is 2.0 Å. (b) Diffraction pattern NqrC_{33–257} with the short side oriented to the beam showing well defined spots to 1.7 Å resolution. (c) Diffraction pattern of the same crystal of NqrC_{33–257} rotated 90° compared with the orientation in (b). When the beam crosses the long side of the crystal smeared spots and a lower diffraction limit were observed.

Table 2

Data-collection and refinement statistics for NqrC_{33–257}.

Values in parentheses are for the outer shell.

Crystal	Native	Native, truncated data
X-ray source	X06SA HR, SLS	
Wavelength (Å)	1.0	
Detector	Dectris PILATUS 6M	
Total rotation range (°)	720	304
Resolution range (Å)	50–1.7 (1.8–1.7)	50–1.7 (1.8–1.7)
Space group	<i>P</i> 2 ₁	
Unit-cell parameters (Å, °)	<i>a</i> = 46.7, <i>b</i> = 41.7, <i>c</i> = 61.4, β = 107.7	
No. of reflections	287190 (24799)	136521 (18406)
No. of unique reflections	25409 (3971)	22276 (3584)
Multiplicity	11.3 (6.2)	6.1 (5.1)
$\langle I/\sigma(I) \rangle$	10.3 (1.2)	11.4 (1.2)
Completeness (%)	99.9 (99.8)	88.1 (90.8)
<i>R</i> _{merge} (%)	15.5 (182)	9.4 (134)
<i>R</i> _{meas} (%)	16.2 (198)	10.2 (149)
CC _{1/2}	99.8 (74.1)	99.8 (53.2)
No. of molecules per asymmetric unit	1	
Matthews coefficient (Å ³ Da ⁻¹)	2.34	
Solvent content (%)	47.5	
<i>R</i> _{work} (%)	18.4 (37.5)	
<i>R</i> _{free} (%)	20.9 (39.6)	
Average <i>B</i> factors (Å ²)		
All atoms	39.2	
Protein	38.8	
Solvent	43.6	

We thank the staff of beamlines X06SA and X06DA at the SLS for excellent support. This work was supported by contract research ‘Methoden in den Lebenswissenschaften’ of the Baden-Württemberg Stiftung P-LS-Meth/4 (to HMM, JS and GF) and by Deutsche Forschungsgemeinschaft grant FR 1321/3-1 (to JS) and grant FR 1488/3-2 (to GF). HMM and GF would like to acknowledge funding by the Young Scholar Fund of the University of Konstanz.

References

Adams, P. D. *et al.* (2010). *Acta Cryst.* **D66**, 213–221.

- Afonine, P. V., Grosse-Kunstleve, R. W., Echols, N., Headd, J. J., Moriarty, N. W., Mustyakimov, M., Terwilliger, T. C., Urzhumtsev, A., Zwart, P. H. & Adams, P. D. (2012). *Acta Cryst.* **D68**, 352–367.
- Basters, A., Geurink, P. P., Oualid, F. E., Ketscher, L., Casutt, M. S., Krause, E., Ovaa, H., Knobeloch, K. P. & Fritz, G. (2014). *FEBS J.* **281**, 1918–1928.
- Bertsova, Y. V., Fadeeva, M. S., Kostyrko, V. A., Serebryakova, M. V., Baykov, A. A. & Bogachev, A. V. (2013). *J. Biol. Chem.* **288**, 14276–14286.
- Casutt, M. S., Nediakov, R., Wendelspiess, S., Vossler, S., Gerken, U., Murai, M., Miyoshi, H., Möller, H. M. & Steuber, J. (2011). *J. Biol. Chem.* **286**, 40075–40082.
- Casutt, M. S., Schlosser, A., Buckel, W. & Steuber, J. (2012). *Biochim. Biophys. Acta*, **1817**, 1817–1822.
- Casutt, M. S., Wendelspiess, S., Steuber, J. & Fritz, G. (2010). *Acta Cryst.* **F66**, 1677–1679.
- Cowtan, K. (2006). *Acta Cryst.* **D62**, 1002–1011.
- DiMaio, F., Echols, N., Headd, J. J., Terwilliger, T. C., Adams, P. D. & Baker, D. (2013). *Nature Methods*, **10**, 1102–1104.
- Duffy, E. B. & Barquera, B. (2006). *J. Bacteriol.* **188**, 8343–8351.
- Emsley, P. & Cowtan, K. (2004). *Acta Cryst.* **D60**, 2126–2132.
- Eswar, N., Webb, B., Marti-Renom, M. A., Madhusudhan, M. S., Eramian, D., Shen, M.-Y., Pieper, U. & Sali, A. (2006). *Curr. Protoc. Bioinformatics*, Unit 5.6, doi:10.1002/0471250953.bi0506s15.
- Grosse-Kunstleve, R. W. & Adams, P. D. (2003). *Acta Cryst.* **D59**, 1966–1973.
- Häse, C. C. & Mekalanos, J. J. (1999). *Proc. Natl Acad. Sci. USA*, **96**, 3183–3187.
- Kabsch, W. (2010). *Acta Cryst.* **D66**, 125–132.
- Karplus, P. A. & Diederichs, K. (2012). *Science*, **336**, 1030–1033.
- Kelley, L. A. & Sternberg, M. J. (2009). *Nature Protoc.* **4**, 363–371.
- Kleywegt, G. J., Zou, J. Y., Kjeldgaard, M. & Jones, T. A. (2001). *International Tables for Crystallography*, Vol. F, edited by M. G. Rossmann & E. Arnold, pp. 353–356, 366–367. Dordrecht: Kluwer Academic Publishers.
- Langer, G., Cohen, S. X., Lamzin, V. S. & Perrakis, A. (2008). *Nature Protoc.* **3**, 1171–1179.
- McCoy, A. J., Grosse-Kunstleve, R. W., Adams, P. D., Winn, M. D., Storoni, L. C. & Read, R. J. (2007). *J. Appl. Cryst.* **40**, 658–674.
- Murshudov, G. N., Skubák, P., Lebedev, A. A., Pannu, N. S., Steiner, R. A., Nicholls, R. A., Winn, M. D., Long, F. & Vagin, A. A. (2011). *Acta Cryst.* **D67**, 355–367.
- Nediakov, R., Steffen, W., Steuber, J. & Möller, H. M. (2013). *J. Biol. Chem.* **288**, 30597–30606.
- Tao, M., Türk, K., Diez, J., Grütter, M. G., Fritz, G. & Steuber, J. (2006). *Acta Cryst.* **F62**, 110–112.
- Terwilliger, T. (2004). *J. Synchrotron Rad.* **11**, 49–52.
- Türk, K., Puhar, A., Neese, F., Bill, E., Fritz, G. & Steuber, J. (2004). *J. Biol. Chem.* **279**, 21349–21355.
- Zhang, K. Y. J., Cowtan, K. & Main, P. (1997). *Methods Enzymol.* **277**, 53–64.